Detection of Artificial Air Space Opacities with Digital Radiography: Ex Vivo Study on Enhanced Latitude Post-Processing

Detektion artifizieller alveolärer Verschattungen in der digitalen Übersichtsradiografie: Ex-vivo-Studie zur Bildnachverarbeitung mit erweiterter Latitude

Autoren

J. Biederer[1], H. Bolte[1], T. Schmidt[1], N. Charalambous[1], M. Both[1], U. Kopp[2], B. Hoffmann[1], S. Freitag-Wolf[3], R. Van Metter[4], M. Heller[1]

Institute

[1] Klinik für Diagnostische Radiologie, Universitätsklinikum Schleswig-Holstein, Campus Kiel
[2] Stralsund, Gemeinschaftspraxis für Radiologie
[3] Institut für Medizinische Informatik und Statistik, Universitätsklinikum Schleswig-Holstein Campus Kiel
[4] private

Key words
- thorax
- digital radiography
- infection

eingereicht 17.8.2009
akzeptiert 23.11.2009

Bibliografie
DOI http://dx.doi.org/10.1055/s-0028-1109961
Online-Publikation: 22.1.2010
Fortschr Röntgenstr 2010; 182: 235 – 242 © Georg Thieme Verlag KG Stuttgart · New York · ISSN 1438-9029

Korrespondenzadresse
Prof. Jürgen Biederer
Klinik für Diagnostische Radiologie, Universitätsklinikum Schleswig-Holstein, Campus Kiel
Arnold-Heller-Straße 3, Haus 23
24105 Kiel
Germany
Tel.: ++ 49/4 31/5 97 31 53
Fax: ++ 49/4 31/5 97 31 51
juergen.biederer@rad.uni-kiel.de

Zusammenfassung

Ziel: Untersuchung an a.-p. Radiografien der Lunge in einem Ex-vivo-System, ob die diagnostische Treffsicherheit für alveoläre Verschattungen in den vom Zwerchfell überlagerten Anteilen der Lunge durch Nachberechnung mit erweiterter Latitude und verstärktem Detailkontrast (EVP) verbessert wird.

Material und Methoden: 19 Lungenpräparate von Schlachtschweinen wurden in einem Thoraxphantom mit trachealer Instillation von 20 – 50 ml Gelatine-stabilisierter Flüssigkeit präpariert und direktradiografisch untersucht (3,0 × 2,5 k Detektor/125 kVp/4 mAs). 276 a.-p. Aufnahmen mit und ohne EVP von 1,0 – 3,0 wurden 6 Beobachtern präsentiert. 8 Regionen wurden für alveoläre Verschattungen bewertet, Referenz war ein separat ausgewertetes CT. Die statistische Auswertung umfasste Sensitivität/Spezifität, Interobserver-Variabilität und eine ROC-Analyse.

Ergebnisse: In den vom Zwerchfell abgedeckten Lungenanteilen (32/92 Regionen verschattet) verbesserte sich der Median der Sensitivität von 0,35 ohne EVP auf 0,53 – 0,56 bei EVP 1,5 – 3,0 (signifikant bei 5/6 Beobachtern). Die Spezifität verringerte sich von 0,96 zu 0,90 (signifikant bei 6/6), Az und Interobserver-Korrelation verbesserten sich von 0,66 nach 0,74 bzw. 0,39 nach 0,48. In nicht überlagerten Lungenabschnitten (136/276 Regionen verschattet) verbesserte sich der Median der Sensitivität von 0,71 auf 0,77 – 0,82 mit EVP (signifikant bei 4/6 Beob.). Spezifität und Az-Wert verringerten sich von 0,76 auf 0,62 und 0,74 auf 0,70 (signifikant bei 3/6).

Schlussfolgerung: Im Ex-vivo-Versuch verbessert EVP die Treffsicherheit für den Nachweis von alveolären Verschattungen in vom Zwerchfell überlagerten Anteilen der Lunge (Fläche unter der ROC-Kurve). In den nicht überlagerten Anteilen geht die verbesserte Sensitivität mit einem Verlust an Spezifität einher.

Abstract

Purpose: To evaluate in a.-p. digital chest radiograms of an ex vivo system if increased latitude and enhanced image detail contrast (EVP) improve the accuracy of detecting artificial air space opacities in parts of the lung that are superimposed by the diaphragm.

Materials and Methods: 19 porcine lungs were inflated inside a chest phantom, prepared with 20 – 50 ml gelatin-stabilized liquid to generate alveolar air space opacities, and examined with direct radiography (3.0 × 2.5 k detector/125 kVp/4 mAs). 276 a.-p. images with and without EVP of 1.0 – 3.0 were presented to 6 observers. 8 regions were read for opacities, the reference was defined by CT. Statistics included sensitivity/specificity, interobserver variability, and calculation of Az (area under ROC curve).

Results: Behind the diaphragm (opacities in 32/92 regions), the median sensitivity increased from 0.35 without EVP to 0.53 – 0.56 at EVP 1.5 – 3.0 (significant in 5/6 observers). The specificity decreased from 0.96 to 0.90 (significant in 6/6), and the Az value and interobserver correlation increased from 0.66 to 0.74 and 0.39 to 0.48, respectively. Above the diaphragm, the median sensitivity for artificial opacities (136/276 regions) increased from 0.71 to 0.77 – 0.82 with EVP (significant in 4/6 observers). The specificity and Az value decreased from 0.76 to 0.62 and 0.74 to 0.70, respectively, (significant in 3/6).

Conclusion: In this ex vivo experiment, EVP improved the diagnostic accuracy for artificial air space opacities in the superimposed parts of the lung (area under the ROC curve). Above the diaphragm, the accuracy was not affected due to a tradeoff in sensitivity/specificity.

Introduction

Over the past decade, digital radiography has continued to replace conventional film-screen radiography of the chest [1]. Storage phosphor image receptors and flat panel detectors not only match the quality of the former technique but also open possibilities for overcoming traditional limitations [2]. One significant challenge are the major differences in X-ray transmittance of the thorax. Systematic studies showed that conventional X-ray films with optimum contrast in mid-density areas frequently fail to provide adequate diagnostic quality in the apices, the retro-cardiac region and behind the diaphragm due to underexposure [3, 4]. Current solutions including wide-latitude films, dual image receptor screen-film combinations or fixed or flexible compensation filters placed close to the source of the X-rays are either achieved at the cost of a considerable loss in edge contrast or are technically complicated and expensive [5–7].

Digital systems cover a much wider range of exposures than a conventional film. However, frequently the old contrast/latitude trade-off is re-introduced when a limited range of exposures is selected from the raw data to display diagnostic images that look like a conventional film radiogram. Additional information poorly displayed on the far tails of the display curve is then sacrificed. Hence, different post-processing techniques to widen the dynamic range of digital images have been developed [8–11]. EVP (enhanced visualization processing, Carestream Health, Inc., Rochester, NY, USA) as one example, separately reduces the contrast of the low image frequencies, thereby increasing the latitude [8, 12]. Simultaneously, the high frequencies are enhanced to preserve detail contrast. It was hypothesized that latitude enhancement of digital projection images would improve the detection of artificial air space opacities behind the diaphragm, without significant effects on other regions. The objective of this study was to perform an ex vivo experiment with EVP as one of the current equalization post-processing techniques to determine whether it could enhance the accuracy of the detection of artificial air space opacities in parts of the lung that are superimposed by the diaphragm.

Materials and Methods

The ex vivo setup

The “artificial thorax” consists of a double-walled container holding a freshly excised, inflated porcine heart-lung explant [13, 14]. The artificial chest walls have a thickness of 2–5 cm and are filled with saline to achieve realistic X-ray absorbency. The silicone “diaphragm” was filled with water. 19 lung specimens were harvested from regular-weight pigs (80–100 kg) at a local slaughterhouse. No animals were sacrificed for the purposes of this study. A 6.5 mm tracheal tube (Portex; SIMS Portex Ltd., Hythe, Kent, UK) was introduced into the trachea and connected to an outlet through the phantom wall. The lungs were then inflated by continuous evacuation of the artificial pleural space at –20 to –30 hPa. Lung collapse and shifting during transfer from CT to the X-ray unit were prevented by maintaining the evacuation. For chest X-ray the phantom was collocated onto a wooden support (**Fig. 1**).

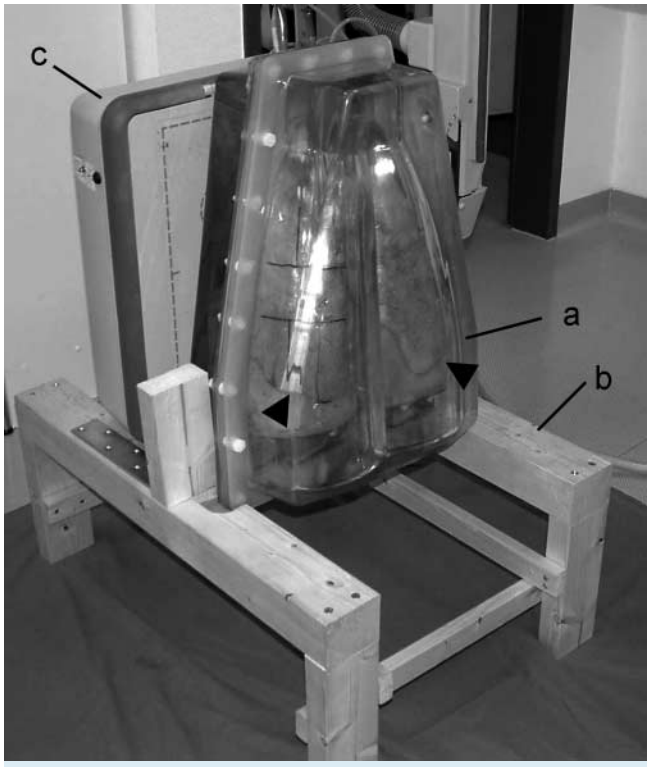

Fig. 1 For chest X-ray studies, the artificial thorax **a** was collocated onto a wooden support **b** in an upright position. This made it possible to take chest X-ray exposures with the direct radiography detector **c** as in patient studies. Lung collapse was prevented by keeping the system constantly evacuated during positioning. The margins of the lung inside the posterior recesses are indicated by black arrow heads.

Abb. 1 Für die digitale Direktradiografie wie an einem stehenden Patienten wurde das Thoraxphantom **a** auf einem Holzgestell **b** in aufrechter Position fixiert. Der Kollaps der Lungen während der Positionierung wurde durch einen konstanten Unterdruck im künstlichen Pleuraspalt verhindert. Die Lungengrenzen in den posterioren Zwerchfellrippenwinkeln sind mit schwarzen Pfeilspitzen markiert

Simulation of artificial air space opacities

Each of the 19 lungs was prepared with simulated pulmonary opacities by injecting 30–50 ml of a gelatin-stabilized liquid into the tracheobronchial system (7.5 g of cold prepared food gelatin (Homann, Dissen, Germany) per 100 ml of water (aqua ad injectabilia, Braun, Melsungen, Germany) [14]). Gelatin served to increase the viscosity and to prevent fast drying. To achieve distribution into the distal air spaces, the evacuation was temporarily interrupted to deflate the lungs. Then the liquid was instilled via a soft silicone tube during re-inflation of the lung explants. The sites of liquid deposition included areas in the posterior costophrenic angles (superimposed by the artificial diaphragm) and areas above the diaphragmatic dome (non-superimposed). Per definition from the latest guidelines of the Fleischner Society, the generated fluid accumulations inside the air spaces are referred to as artificial air space opacities rather than infiltrates [15].

Computed tomography and documentation of findings

Injection of the liquid was carried out on top of the CT table of a commercial 16-row detector scanner (Sensation 16, Siemens Healthcare, Erlangen, Germany). CT scans with a standard chest protocol were acquired prior to and after the injection

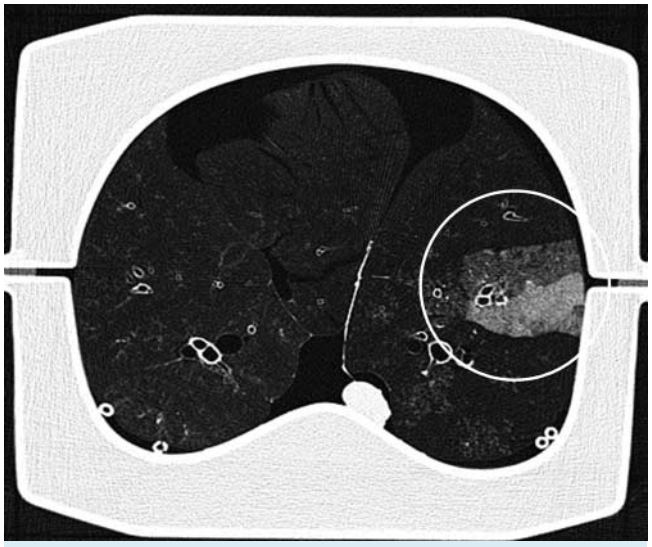

Fig. 2 CT cross section just above the diaphragm showing a dense artificial air space opacity in the lateral left lower lobe (circled). Nb.: Chest tubes in the posterior recesses for the evacuation of the artificial pleural space.

Abb. 2 CT-Querschnitt unmittelbar oberhalb der Zwerchfellkuppe mit Abbildung einer dichten intraalveolären Verschattung im lateralen linken Lungenunterlappen (Kreis). Nb.: Drainagen in den posterioren Abschnitten zur Absaugung der Luft aus dem künstlichen Pleuraspalt.

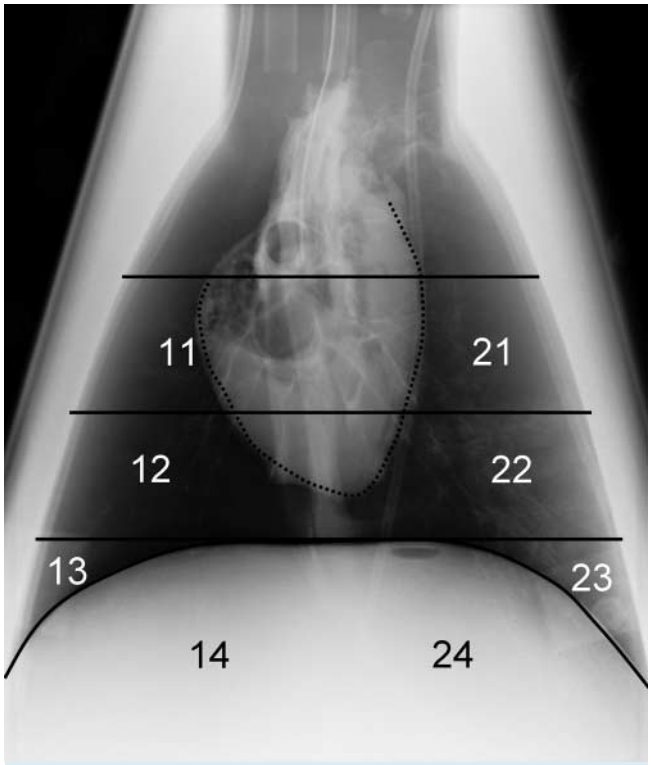

Fig. 3 Standard tone scale image of the phantom taken at 4 mAs, 125 kVp. The grid indicates the margins of the 8 regions that were read for the presence of air space opacities (the same lung as in Fig. **2**).

Abb. 3 Aufnahme des Phantoms mit 4 mAs, 125 keV, Nachverarbeitung mit der Standard-Grauwertskala. Die überlagerten Linien zeigen die Grenzen der 8 Regionen, die für das Vorhandensein von Verschattungen bewertet wurden (gleiche Lunge wie in **Abb. 2**).

(100 mAs, 120 kVp, slice collimation 16 × 0,75 mm, table feed 15 mm, reconstructed slice thickness 1 mm, reconstruction increment 0.7 mm, B70f kernel, FOV 350 mm, matrix 512 × 512 pixel). The location of the artificial air space opacities was recorded by two board certified radiologists using a standard display (window width 1600 HU, center at –600 HU) on a commercial workstation (CT WIZARD®, syngoCT, Siemens Healthcare, Erlangen, Germany; ▶ **Fig. 2**). Documentation was produced for eight regions of the image defined by lines at the level of the carina, mid-way between carina/diaphragm and at the diaphragmatic dome. The area below the top of the diaphragmatic dome was divided into the non-superimposed lateral recesses and the parts that were superimposed by the hemidiaphragm. Finally, each region was divided by the midline into a right (numbered from 11 – 14) and left section (numbered from 21 – 24; ▶ **Fig. 3**). The retrocardium was excluded since the position of the heart was variable. To match CT and radiography, the scout view of the CT and the radiograms were compared side by side. These data served as the gold standard.

Digital radiography and image post-processing

The direct radiography system (KODAK DIRECTVIEW DR 9000 System, Rochester, NY, USA) was equipped with a 35 × 43 cm flat panel detector consisting of an amorphous selenium semiconductor X-ray absorber coating over a thin-film transistor array of amorphous silicon. The matrix of 2560 × 3072 elements corresponded to a single pixel size of 139 µm. The image bit depth was 14. All images were acquired in the postero-anterior projection at a distance of 180 cm at 125 kVp, once with a fixed time-current product of 4 mAs and once with automatic exposure control (cut-off dose for the detector was set to 4 µGy). This was compliant with the 5 µGy detector dose limit for 400 speed systems defined by law in the country where the study was performed. The fixed 4 mAs images were further processed for the study. The average tube load with automatic exposure was only obtained as a measure of the phantoms overall X-ray transmittance (4.49 mAs ± SD 0.61). For comparison, we retrospectively analyzed the average tube load from automatic exposures in 70 consecutive routine examinations of the same unit (3.88 mAs ± SD 1.04 for adult male patients). Raw image data (2456 × 2968 pixel) for each image was archived to CD-ROM and transferred to a personal computer equipped with a copy of the fully functional image processing software of the DR unit.

Radiographies without EVP post-processing were produced with the default automated tone scale algorithm of the Kodak DirectView systems. It is based on a “perceptually linear” tone scale that properly incorporates the characteristics of the human visual system [16 – 18]. The essential elements of the algorithm, i. e., image analysis, tone scale generation, and tone scale application, produce a display-ready image that is similar in appearance to optimum screen-film imaging [19]. The purpose of enhanced visualization processing (EVP) is to increase the latitude of radiographic images while preserving or enhancing the contrast of image detail.

Latitude is defined as the difference between the lowest and the highest exposure value covered by the grayscale of the image. Exposures below this window are displayed in white, exposures above in black tones. This is accomplished by analyzing the image as low and high-frequency component images. The contrast of the low-frequency image is reduced, thereby increasing the latitude (range of exposures visible in the im-

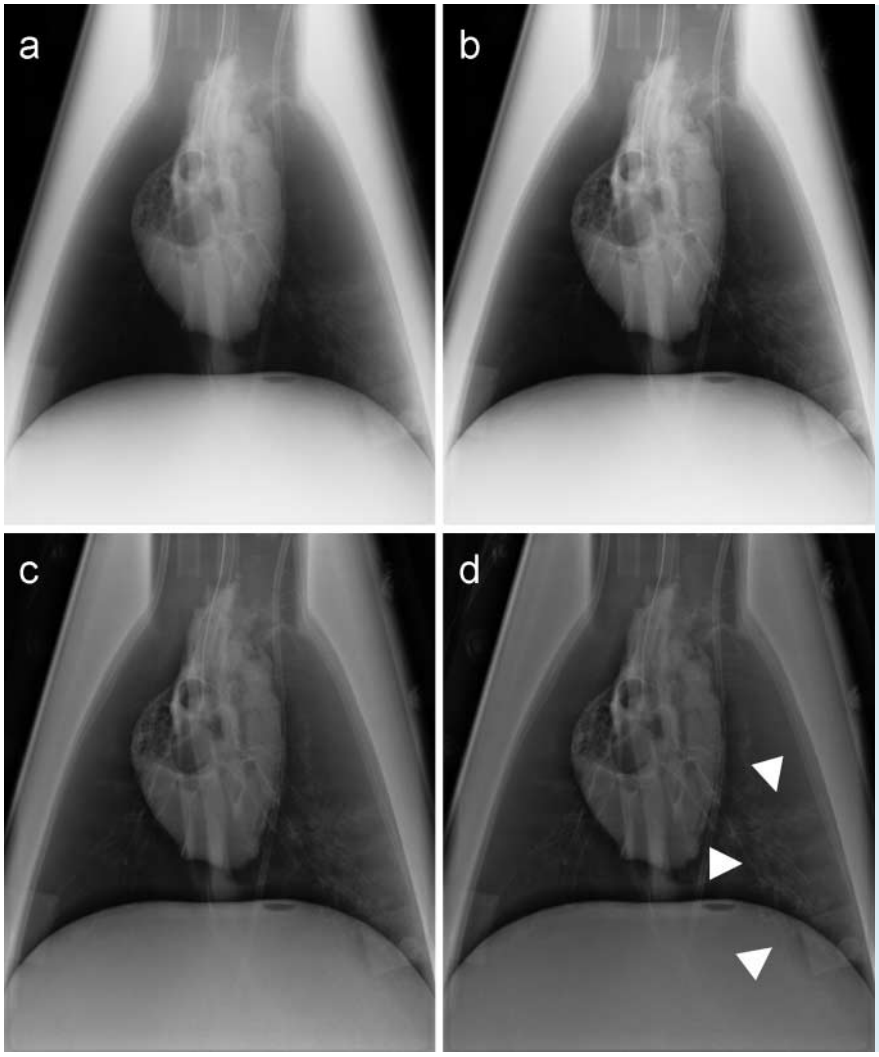

Fig. 4 Example demonstrating the effects of image post-processing with increased latitude on an image of the phantom taken at 4 mAs, 125 kVp (same lung as in **Fig. 2, 3**). The artificial air space opacity in the lateral left lower lobe (indicated by white arrow heads in image **d**) is hardly visible at standard tone scale **a** and becomes clearly visible with increased latitude with log.-factors of 1.0 **b**, 2.0 **c** and 3.0 d. The difference between **c** and **d** is only marginal.

Abb. 4 Ein Beispiel zur Demonstration der Bildnachverarbeitung mit erweiterter Latitude an einer Aufnahme bei 4 mAs und 125 keV (gleiche Lunge wie in **Abb. 2, 3**). Die artifiziellen intraalveolären Verschattungen im lateralen linken Lungenunterlappen (markiert mit weißen Pfeilspitzen in **d**) sind bei Nachverarbeitung mit der Standard-Grauwertskala schwer erkennbar **a**, demarkieren sich aber deutlicher mit Erweiterung der Latitude um Log.-Faktoren von 1,0 **b**, 2,0 **c** und 3,0 d. Hierbei ist der Unterschied zwischen **c** und **d** nur noch marginal.

age). The contrast of the high-frequency image may be enhanced to preserve the visual appearance of image detail. Finally, the altered low- and high-frequency image components are recombined and the tone scale mapping is applied. Hence the effect of EVP is to lower the overall or global contrast of the image, thereby increasing the latitude of the displayed image. In this way image features that would have been very light or very dark are made darker or lighter, respectively. In addition, the contrast of image details smaller than the kernel size is increased. EVP thus extends the latitude of the displayed image, without any loss of contrast for details at mid-range exposures. A larger fraction of the potentially useful diagnostic information is presented without the need for image manipulation by the radiologist. For a detailed description of the technique, refer to [8, 12].

In this study, renderings of each image were prepared with the default automated tone scale algorithm as well as with five levels of latitude enhancement having EVP gain values (α-1) from 1.0 to 3.0 in increments of 0.5. An EVP gain of 2.0 doubles the latitude of an image. The EVP kernel size was set to the manufacturer's default value for chest imaging, 1/20 of the short dimension of the image (17.5 mm). The high-frequency gain (β) in these experiments was set to the recommended default of 1.1. The images were extracted in six different processing conditions and saved for review as DICOM files (**Fig. 4**). Then the original image was mirrored in left-right direction and another set of six images was produced. These mirrored images were included to reduce recall bias since all images appeared six times with different image processing conditions. Additional X-rays were obtained prior to the injection of liquid in 4 of 19 lungs and included as negative controls. Thus, a total of 23 acquisitions and a total of 276 rendered images were available for reading.

Image reading

The images were presented in a room with low ambient lighting on the diagnostic 1280 × 1024 pixel TFT monitor of a commercial workstation (monitor: SMD 1879-M, Siemens, Erlangen, Germany; graphic processor: Matrox Millennium G450 DVI, Matrox Graphics, Dorval, Quebec, Canada; standard viewing software: Magic View 300, Siemens, Erlangen, Germany; monitor calibration for grayscale display was performed by visual assessment of display bit-depth with the TG18-MP pattern of the AAPM (American Association of Physicists in Medicine TG#18). All images appeared individually in randomized order and in full size on a black background with fixed default window settings of 2048 (center)/4095 (width). The initially fixed monitor settings and ambient light were kept constant throughout the study. The images were randomized and presented to six independent observers who were familiar with

Table 1 Results from 23 CT scans (19 of 23 after generation of artificial air space opacities). The table contains the totaled results for all regions (left column) and separately for regions behind the diaphragm (middle) and above the diaphragm (right; for the definition of regions **Fig. 3**). NB: The number of regions in **Table 2** is twice the number in this table since all radiograms were presented twice: one time as original, one time mirrored.

Tab. 1 Ergebnisse aus 23 CT-Datensätzen (19 von 23 nach Erzeugung artifizieller intraalveolärer Verschattungen). Die Tabelle enthält die Gesamtzahl der Ergebnisse für alle Regionen (linke Spalte) sowie getrennt für die Regionen hinter der Zwerchfellkuppe (in der Mitte) und oberhalb der Zwerchfellkuppe (rechts; zur Definition der Regionen **Abb. 3**). Nb.: Die **Tab. 2** weist eine 2-fach höhere Anzahl an Regionen auf, da die Röntgenaufnahmen 2-fach präsentiert wurden (im Original und um die Längsachse gespiegelt).

n = 184	total (regions 11 – 14 and 21 – 24; n = 184)		superimposed by the diaphragm (regions 14 and 24; n = 46)		not superimposed by the diaphragm (regions 11 – 13 and 21 – 23; n = 138)	
	no opacification	air space opacity	no opacification	air space opacity	no opacification	air space opacity
no atelectasis	85	84	22	16	63	68
atelectasis	11	4	6	2	5	2

chest X-ray reading from the daily routine (2, 2, 3, 4, 6 and 8 years of chest radiology experience, respectively).

The images were read for the presence or absence of opacifications in the above defined regions. To reduce the learning bias, the readers were instructed during a separate session with 25 training images and subsequent presentation of the correct information (these images were not presented again in the main study). Reading time was limited to 6 min per image and four hours per day. Breaks could be taken whenever desired, but at least every hour for 10 min.

Statistics

The sensitivity and specificity for the artificial air space opacities were calculated. The six regions 11 – 13 and 21 – 23 were regarded as representative of non-superimposed lung parenchyma above the diaphragm, while the two regions 14 and 24 represented the superimposed parts of the lung (anterior and posterior pleural recesses, **Fig. 2**). The significance of different latitude levels upon sensitivities and specificities for each individual reader was calculated with McNemar's test. A p-value of 0.05 was defined as statistically significant. For statistical evaluation of diagnostic accuracy, the results for sensitivities and specificities were averaged over the six readers. As suggested by van den Hout, the mean sensitivity and specificity at different processing levels were summarized as Az = 1/2 (sensitivity + specificity), which corresponds to the area under an ROC curve with a single data point (non-parametric calculation/trapezoidal rule under the assumption of a concave receiver operating characteristic (ROC) curve) [20, 21]. Positive and negative predictive values were not calculated since according to Bayes' theorem they depend on the incidence of a finding and could be manipulated in the experiment. Interobserver agreement was described with Cohen's kappa. A kappa value smaller that 0.10 was rated as no agreement (0.10 – 0.40 "weak", 0.41 – 0.60 "moderate" and 0.61 – 0.80 "good" agreement). A correlation of results with the density of findings on CT was not performed since this data was only descriptive. Calculations were made with standard software (Excel 97, Microsoft, Redmond, WA, USA; SPSS, 10.0, SPSS Inc., Chicago, IL, USA).

Results

Radiographic presentation of the artificial air space opacities

The radiographic presentation of the opacifications varied from dense and easily detectible to very fine, almost invisible attenuations. This corresponded to the appearance in CT where diffuse, confluent and dense opacifications were seen at segmental and subsegmental levels. 23 CT scans, each with 8 subregions were included in the statistical evaluation. Of the resulting 184 subregions, 84 presented with opacifications, 11 were partially collapsed (characterized as atelectasis) and 4 had both partial atelectasis and artificial air space opacities. 85 subregions presented without any finding. For the distribution of findings behind and above the diaphragm, refer to **Table 1**.

Accuracy of detecting artificial air space opacities in superimposed parts of the lung

The diagnostic accuracy for the detection of artificial air space opacities in superimposed parts of the lung behind the diaphragm was calculated from 3312 single observations (n = 92 regions, each presented at six latitude levels and read by six observers. For details, see the left section of **Table 2** and **Fig. 5a**). Behind the diaphragm (artificial air space opacities present in 32/92 regions), the median sensitivity for artificial air space opacities improved from 0.35 over 0.50 at a latitude enhancement gain of 1.0 (changes not significant) to 0.56 at a gain of 3.0 (changes significant in 3 of the 6 observers). The specificity remained almost unchanged around 0.95 for latitude enhancement gains of up to 2.0, but decreased to 0.90 at a gain of 3.0 (changes compared to the standard tone scale significant in 3 of 6 observers). The Az values improved from 0.66 at the standard tone scale to 0.73 – 0.74 at any level of enhanced latitude post-processing. The difference with respect to the median Az at the standard tone scale was significant at all levels. Interobserver agreement improved from 0.39 to a maximum of 0.48 at a gain of 1.0 (**Table 3**). A further increase in latitude resulted in median kappa values between 0.40 and 0.46 (individual values ranging from 0.32 – 0.55, changes not significant).

Accuracy of detecting artificial air space opacities in non-superimposed parts of the lung

The calculation of diagnostic accuracy for the detection of artificial air space opacities in non-superimposed parts of the lung (above the diaphragm) was based on 9936 single observations (n = 276 regions, each presented at six latitude levels and read by six observers, opacifications present in 136/276 regions. For details, see the right section of **Table 2** and **Fig. 5b**). Within this group, the median sensitivity for artificial air space opacities increased from 0.71 on standard tone scale images over 0.77 with latitude enhancement at a gain of 1.0 to 0.82

Table 2 Diagnostic accuracy for the detection of artificial air space opacities behind the diaphragm (3312 single observations from 46 images, n = 92 regions, six latitude levels and six observers) and above (9936 single observations from 46 images, n = 276 regions, six latitude levels and six observers). The median of the observers appears in italic type, and the range of the individual results and the fraction of observers with significant changes compared to the standard tone scale appear in brackets.

Tab. 2 Diagnostische Treffsicherheit für die Detektion artifizieller intraalveolärer Verschattungen hinter dem Zwerchfell (3312 Einzelbeobachtungen der 6 Beobachter an 46 Aufnahmen für 92 Regionen und 6 Stufen der Latitudenerweiterung) und oberhalb der Zwerchfellkuppe (9936 Einzelbeobachtungen der 6 Beobachter an 46 Aufnahmen für 276 Regionen und 6 Stufen der Latitudenerweiterung). Der jeweilige Median der Beobachter ist in Kursivdruck wiedergegeben, die Spannweite der individuellen Ergebnisse und der Anteil der Beobachter mit signifikant von der Standard-Grauwertskala abweichenden Ergebnissen in runden Klammern.

latitude	behind diaphragm (n = 92 regions)			above diaphragm (n = 276 regions)		
level	sensitivity	specificity	Az	sensitivity	specificity	Az
	median (range)	median (range)		median (range)	median (range)	
0	*0.35* (0.14 – 0.64)	*0.96* (0.84 – 0.98)	*0.66*	*0.71* (0.60 – 0.75)	*0.76* (0.66 – 0.84)	*0.74*
1	*0.50* (0.33 – 0.72; 0 / 6 sign.)	*0.95* (0.86 – 1.00; 1 / 6 sign.)	*0.73*	*0.77* (0.72 – 0.85; 3 / 6 sign.)	*0.70* (0.50 – 0.78; 2 / 6 sign.)	*0.74*
1.5	*0.53* (0.42 – 0.94; 3 / 6 sign.)	*0.95* (0.81 – 1.00; 1 / 6 sign.)	*0.74*	*0.75* (0.72 – 0.88; 3 / 6 sign.)	*0.64* (0.30 – 0.76; 3 / 6 sign.)	*0.70*
2	*0.51* (0.47 – 0.94; 4 / 6 sign.)	*0.95* (0.77 – 0.96; 1 / 6 sign.)	*0.73*	*0.81* (0.76 – 0.87; 5 / 6 sign.)	*0.64* (0.30 – 0.79: 6 / 6 sign.)	*0.73*
2.5	*0.54* (0.40 – 0.92; 4 / 6 sign.)	*0.91* (0.73 – 0.96; 2 / 6 sign.)	*0.73*	*0.81* (0.76 – 0.89; 5 / 6 sign.)	*0.64* (0.30 – 0.79; 5 / 6 sign.)	*0.73*
3	*0.56* (0.50 – 0.92; 3 / 6 sign.)	*0.90* (0.73 – 0.98; 3 / 6 sign.)	*0.73*	*0.82* (0.78 – 0.91; 5 / 6 sign.)	*0.62* (0.28 – 0.78; 5 / 6 sign.)	*0.72*

Table 3

Tab. 3

EVP	interobserver kappa	
median range		
behind diaphragm		
off	*0.39*	0.27 – 0.52
1.0	*0.48*	0.38 – 0.59
1.5	*0.46*	0.38 – 0.55
2.0	*0.46*	0.38 – 0.54
2.5	*0.40*	0.32 – 0.48
3.0	*0.44*	0.37 – 0.52
above diaphragm		
off	*0.55*	0.52 – 0.58
1.0	*0.52*	0.49 – 0.56
1.5	*0.48*	0.44 – 0.52
2.0	*0.44*	0.40 – 0.49
2.5	*0.48*	0.43 – 0.52
3.0	*0.48*	0.44 – 0.53

at a gain of 3.0 (changes compared to the standard tone scale significant in 5 of the 6 observers). The specificity decreased from 0.76 at the standard tone scale over 0.70 with latitude enhancement at a gain of 1.0 to 0.62 at a gain of 3.0 (changes significant in 5 of 6 observers). The Az values ranged from 0.70 to 0.74 and at any level of latitude (changes not significant). Median kappa values for interobserver agreement changed from a maximum of 0.55 at the standard tone scale over 0.52 at a latitude level of 1.0 to 0.44 – 0.48 at a gain of 3.0 (changes not significant). Differences between observers related to chest radiology experience were not observed.

Discussion

The ex vivo study demonstrated that post-processing of digital projection chest radiograms with moderately increased latitude and simultaneously enhanced detail contrast improved the sensitivity for artificial air space opacities, in particular for parts of the lung superimposed by the diaphragm. However, depending on the level of EVP gain, this effect was significant in only 4 of 6 observers. The specificity decreased simultaneously indicating false positive findings. Hence, overall improvement of diagnostic accuracy was registered only for superimposed parts of the lung behind the diaphragm and did not change above the diaphragm. Individual differences in the response to the level of increased latitude were observed. Interobserver agreement for the regions behind the diaphragm improved from standard tone scale to latitude enhancement with a gain of 1.0 but tended to decrease again at higher levels.

As an advantage of the study, the experiment simulated a realistic setting: reading chest X-rays for pulmonary opacities. The necessary raw image data with CT correlation could be easily produced. Comparable clinical data with proven infiltrative lung disease and corresponding CT would have been more difficult to obtain: repeated exposures would have been prohibitive in patients or at least ethically problematic in a laboratory animal [22, 23]. The phantom size, radiation absorption and the dynamic range of X-ray transmittance (which is proportional to the required latitude of the imaging system) were equivalent to those of a large human thorax [13, 14]. This was confirmed by retrospective comparison of the tube loads for adult male patients in automatic exposure control images. By using a fixed exposure of 4 mAs, variations with respect to the position of the phantom and the inserted material were excluded.

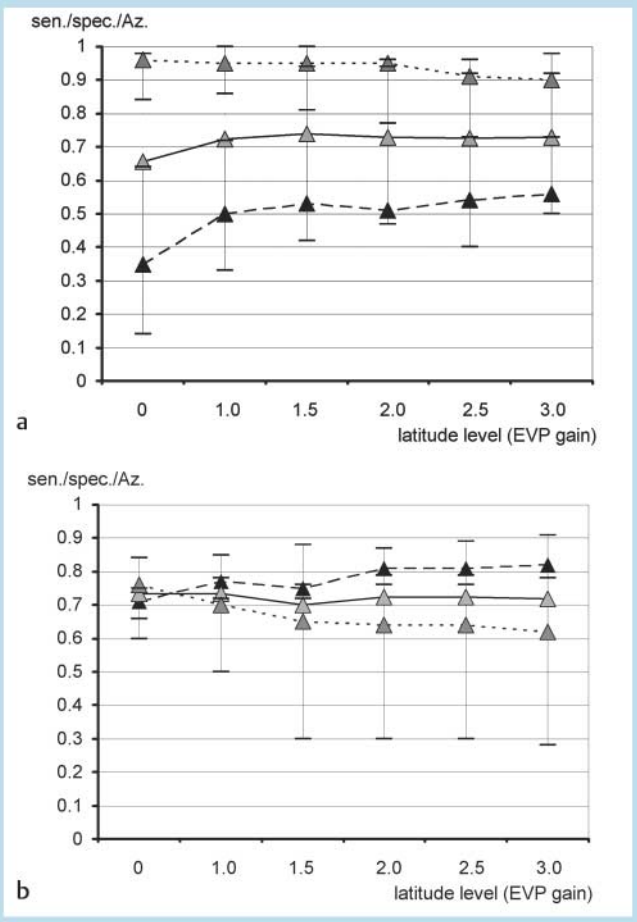

Fig. 5 Graphics demonstrating the contents of **Table 2**: Diagnostic accuracy for the detection of artificial air space opacities behind **a** and above the diaphragm **b**. Black marks and the dotted line represent the median of the sensitivity calculated from the observations of six different readers at given latitude levels from 0 to 3.0. The span of the individual results is indicated by error bars. Accordingly, dark gray marks and corresponding error bars with a dashed line represent the specificity. Light gray marks and the straight line represent the Az values calculated from the medians of sensitivity and specificity.

Abb. 5 Grafische Illustration des Inhalts von **Tab. 2**: Diagnostische Treffsicherheit für die Detektion artifizieller intraalveolärer Verschattungen hinter **a** und über der Zwerchfellblase **b**. Die schwarzen Marken und die gepunktete Linie zeigen den Median der Sensitivität berechnet aus den Aufzeichnungen der 6 Beobachter bei Latituden-Erweiterung von 0 – 3,0. Die Spannweite der Einzelwerte wird durch Fehlerbalken angezeigt. Dunkelgraue Marken mit Fehlerindikator und einer gestrichelten Linie geben die Spezifität wieder. Hellgraue Marken und die durchgezogene Linie entsprechen den Az-Werten (Fläche unter der ROC-Kurve, berechnet aus den Medianwerten für die Sensitivität und Spezifität).

Realistic artificial air space opacities of variable extent and density were produced with gelatin-stabilized liquid [14]. Unlike for pulmonary nodules, electronic simulation of such "infiltrates" was not available [24 – 26]. It was assumed that differences between porcine and human material would not be relevant for the detection of pulmonary opacifications. Multiple row detector CT provided the best available standard for the detection of pulmonary opacifications [27 – 30]. The higher sensitivity of CT for the artificial air space opacities in this experiment is consistent with studies on immunocompromised patients which demonstrated that the sensitivity of chest X-ray for subtle pulmonary infiltrates approximates 50 – 70% [30 – 32]. A realistic amount of anatomic noise was represented [23]. Independent factors such as heart pulsation or attenuations related to the chest wall (ribs and spine) were excluded. The influence of overlying bones could not be studied, but this has already been explicitly assessed by other investigators [23, 25].

Limitations of the study

The presented data should not be interpreted as a measure to quantify differences in the diagnostic accuracy of X-ray and CT, since the density of opacifications was not standardized. The accuracy of detecting air space opacities behind and above the diaphragm was not directly compared since the prevalence of opacifications in both regions differed after exclusion of atelectases (32/92 and 136/276, respectively). Furthermore, the lack of blood inside the lung vessels may have biased the detection results between the superimposed and non-superimposed regions. Theoretically, the lack of a vessel filling might facilitate the detection of opacities in the non-superimposed parts more than in the superimposed parts. The lack of other superimposed structures such as bones and air-filled parts of the bowel in the upper abdomen or even lung scars may have contributed to an overestimation of the effects of detail enhancement as well. These structures would have been displayed with sharper delineation and contrast. This might have reduced the positive effects on the detection of air space opacities. Further investigation of this subject should therefore include chest wall structures, e.g. in an experimental setup using cadavers and superimposed nodules to simulate pathology. A more sophisticated setup should principally allow for imaging in two planes as well [31 – 34]. In clinical practice, the lateral image plane is very helpful for detecting lower lobe infiltrates. However, the design of the phantom was not suitable for lateral projections since the flanges and screws are superimposed on the image. Hence, only posterior-anterior projections were analyzed.

Clinical relevance

Latitude enhancement is a general approach to improving radiograms of subjects with a large dynamic range. Our results are specific to EVP, but other programs (e.g. DRC = dynamic range control processing [9]) produce similar effects. For DRC it was shown that it improves the visibility of tubes and lines superimposed on the mediastinal tissues if applied to bedside images taken with a mobile unit. When used for in-department chest radiography, it was assumed to provide slight advantages in the evaluation of disease in the mediastinum [9, 11]. For the EVP algorithm, this was already shown with ex vivo experiments using artificial pulmonary nodules, but the effects on the detection of subtle opacifications have not yet been studied [12].

An advantage of EVP over other techniques is that it is separately effective on high and low frequency components of the full scale raw image [12]. This makes the difference to simply applying a larger window width to all image components. The resulting modified raw image combines a large latitude with good detail contrast. This image is then subject to further routine processing. Other products, e.g. DRC [9], are applied to image data within the display curve. Principally this data has been already truncated by preprocessing, and the effectiveness of such procedures is potentially limited. DRC and EVP have been commercially introduced and studies on storage phosphor systems have demonstrated their comparable capacity

for displaying chest radiograms with a wide dynamic range [8, 9]. In theory, EVP may enhance image noise by enhancing the high frequencies. This effect was not further evaluated, but may be critical in instances with very high EVP gain.

A clinical application of enhanced latitude post-processing would be to improve softcopy image review by sending original (unprocessed) image data to a review station thereby allowing readers to adjust image latitude and detail contrast interactively [10, 12]. Although processing with recalculation of the images on a dedicated workstation with preset keys would take less than five seconds, it appears questionable whether this additional effort would be accepted as routine in a busy radiological department. In clinical practice, image processing methods with automatic tone scale rendering and latitude and contrast enhancements are accepted for producing display ready hardcopies or minimizing the time required for image manipulation during softcopy reading [35]. These effects on clinical workflow were documented recently [35]. Since the recommendations for the latitude enhancement gain can probably not be directly applied to other products, further studies with other products might be useful.

Finally it was concluded from the present data that image post-processing of digital p.a. chest radiograms with EVP improves the diagnostic accuracy for artificial air space opacities in the superimposed parts of the lung (area under the ROC curve). Above the diaphragm accuracy is not affected due to a trade-off in sensitivity/specificity. For practical use, a moderate EVP gain of 1.5 appears to be suitable for most readers. The positive effect of latitude enhancement on sensitivity became statistically significant for 3/6 observers at a level of 1.5 and the negative effects on specificity became effective for a gain of 1.5 for parts above the diaphragm. Hence, in consistency with other literature, we suggest a latitude enhancement gain between 1.0 and 1.5 to be suitable for most readers [12, 36]. With respect to optimum detectability of pulmonary opacifications without a significant loss in specificity, we recommend not exceeding a level of 1.5.

References

1 *Kotter E, Langer M.* Digital radiography with large-area flat-panel detectors. Eur Radiol 2002; 12: 2562–2570
2 *Beute GH, Flynn MJ, Eyler WR et al.* Chest radiographic image quality: comparison of asymmetric screen-film, digital storage phosphor, and digital selenium drum systems-preliminary study. Radiographics 1998; 18: 745–754
3 *Van Metter R, Lemmers H, Schultze-Kool L.* Exposure latitude for thoracic radiography. Proc SPIE 1992; 165: 52–61
4 *Lemmers HEASJ, Schultze-Kool LJ, Van Elburg H et al.* Low frequency transmission of the chest in an out-patient population: Implications for the AMBER imaging system. Proc SPIE 1990; 1231: 437–441
5 *Logan PM, Tunney T, McCoy CT et al.* Comparison of a new dual characteristic film-screen system (insight) with a standard film-screen system for chest radiology. Br J Radiol 1994; 67: 162–165
6 *Chotas HG, Floyd CE J, Ravin CE.* Film-based chest radiography: AMBER vs asymmetric screen-film systems. Am J Roentgenol 1993; 161: 743–747
7 *Vlasbloem H, Kool LJ.* AMBER: a scanning multiple-beam equalization system for chest radiography. Radiology 1988; 169: 29–34
8 *Van Metter R, Foos D.* Enhanced latitude for digital projection radiography. Proc SPIE 1999; 3658: 468–483
9 *Ikezoe J, Takeuchi N, Kido S et al.* Dynamic range control processing of digital chest images. A clinical evaluation. Acta Radiol 1996; 37: 107–115
10 *Tingberg A, Herrmann C, Lanhede B et al.* Influence of the characteristic curve on the clinical image quality of lumbar spine and chest radiographs. Br J Radiol 2004; 77: 204–215
11 *Freedman MT, Artz DS.* Digital radiography of the chest. Semin Roentgenol 1997; 32: 38–34
12 *Biederer J, Gottwald T, Bolte H et al.* Pulmonary Nodule Detection with digital Projection Radiography: An ex vivo Study on increased Latitude Post-Processing. Eur Radiol 2007; 17: 1089–1100
13 *Biederer J, Heller M.* Artificial Thorax for MR Imaging Studies in porcine Heart-Lung Preparations. Radiology 2003; 226: 250–255
14 *Biederer J, Busse I, Grimm J et al.* Sensitivity of MRI in detecting alveolar Infiltrates: Experimental Studies. Fortschr Röntgenstr 2002; 174: 1033–1039
15 *Hansell DM, Bankier AA, MacMahon H et al.* Fleischner Society: glossary of terms for thoracic imaging. Radiology 2008; 246: 697–722
16 *Lee HC, Daly S, Van Metter R.* Visual optimization of radiographic tone scale. Proc SPIE 1997; 3036: 118–129
17 *Hemminger BM, Johnston RE, Rolland JP et al.* Introduction to the perceptual linearization of video display systems for medical image presentation. J Digital Imaging 1995; 8: 21–34
18 *Blume H.* The ACR/NEMA proposal for a gray-scale display function standard. Proc SPIE 1996; 2707: 344–360
19 *Barski LL, Van Metter R, Foos DH et al.* New automatic tone scale method for computed radiography. Proc SPIE 1998; 3335: 164–178
20 *van den Hout WB.* The area under an ROC curve with limited information. Med Decis Making 2003; 23: 160–166
21 *Hanley J, McNeil B.* The meaning and use of the area under a receiver operating characteristic (ROC) curve. Radiology 1982; 143: 29–36
22 *Schueller-Weidekamm C, Wassermann E, Redl H et al.* Dynamic CT measurement of pulmonary enhancement in piglets with experimental acute respiratory distress syndrome. Radiology 2006; 239: 398–405
23 *Don S, Hildebolt CF, Sharp TL et al.* Computed radiography versus screen-film radiography: detection of pulmonary edema in a rabbit model that simulates neonatal pulmonary infiltrates. Radiology 1999; 213: 455–460
24 *Samei E, Flynn MJ, Eyler WR.* Detection of subtle lung nodules: relative influence of quantum and anatomic noise on chest radiographs. Radiology 1999; 213: 727–734
25 *Yocky DA, Seeley GW, Ovitt TW et al.* Computer-simulated lung nodules in digital chest radiographs for detection studies. Invest Radiol 1990; 25: 902–907
26 *Samei E, Flynn MJ, Peterson E et al.* Subtle lung nodules: influence of local anatomic variations on detection. Radiology 2003; 228: 76–84
27 *Weber C, Maas R, Steiner P et al.* Wertigkeit der digitalen Thoraxaufnahme bei der Detektion von Lungeninfiltraten knochenmarktransplantierter Patienten in der Aplasie. Fortschr Röntgenstr 1999; 171: 294–301
28 *Heussel CP, Kauczor HU, Heussel G et al.* Early detection of pneumonia in febrile neutropenic patients: use of thin-section CT. Am J Roentgenol 1997; 169: 1347–1353
29 *Heussel CP, Kauczor HU, Ullmann AJ.* Pneumonia in neutropenic patients. Eur Radiol 2004; 14: 256–271
30 *Hein PA, Romano VC, Rogalla P et al.* Linear and volume measurements of pulmonary nodules at different CT dose levels – intrascan and interscan analysis. Fortschr Röntgenstr 2009; 181: 24–31
31 *Goo JM, Im JG, Lee HJ et al.* Detection of simulated chest lesions by using soft-copy reading: comparison of an amorphous silicon flat-panel-detector system and a storage-phosphor system. Radiology 2002; 224: 242–246
32 *Yamamura J, Wildberger JE, Nagel HD et al.* High-Resolution-MSCT-Untersuchungen zur Infiltratsuche: Untersuchung einer Dosisreduktion bei immunsupprimierten Patienten. Fortschr Röntgenstr 2009; 181: 549–555
33 *Oschatz E, Prokop M, Scharitzer M et al.* Comparison of liquid crystal versus cathode ray tube display for the detection of simulated chest lesions. Eur Radiol 2005; 15: 1472–1476
34 *Bernhardt TM, Rapp-Bernhardt U, Lenzen H et al.* Diagnostic Performance of a Flat-Panel Detector at Low Tube Voltage in Chest Radiography: A Phantom Study. Invest Radiol 2004; 39: 97–103
35 *Kim JH, Im JG, Han MC et al.* Improved visualization of simulated nodules by adaptive enhancement chest radiography. Acad Radiol 1994; 1: 93–99
36 *Krupinski E, Radvany M, Levy A et al.* Enhanced visualization processing: Effect on workflow. Acad Radiol 2001; 8: 1127–1133